SCIENCE CHINA
Earth Sciences

•RESEARCH PAPER•

September 2022 Vol.65 No.9: 1704–1714
https://doi.org/10.1007/s11430-022-9966-5

A novel method for simultaneous analysis of particle size and mineralogy for Chang'E-5 lunar soil with minimum sample consumption

Kenan CAO[1], Mingtan DONG[2], Zhenbing SHE[1*], Qian XIAO[1], Xinyi WANG[1], Yuqi QIAN[3], Yiheng LI[3], Zaicong WANG[3], Qi HE[3], Xiang WU[3], Keqing ZONG[3], Zhaochu HU[3] & Long XIAO[3]

[1] *State Key Laboratory of Biogeology and Environmental Geology, School of Earth Sciences, China University of Geosciences, Wuhan 430078, China;*
[2] *School of Environmental Studies, China University of Geosciences, Wuhan 430078, China;*
[3] *State Key Laboratory of Geological Processes and Mineral Resources, School of Earth Sciences, China University of Geosciences, Wuhan 430078, China*

Received March 22, 2022; revised June 2, 2022; accepted June 13, 2022; published online June 24, 2022

Abstract The successful return of lunar soil samples from the northern Oceanus Procellarum by the Chang'E 5 (CE-5) mission has provided unprecedented ground-truth information for the previously unexplored region of the Moon. In particular, the particle size and mineral constituents of the CE-5 soil samples are of critical importance to interpret remote sensing data. With a Raman-based particle analysis system, we show that the particle size properties and mineral constituents of the CE-5 soil can be simultaneously determined with a small sample size (*ca*. 30 μg). The CE-5 sample scooped from the lunar surface has an overall small size between 0.4 μm and 73.9 μm (mean=3.5 μm), and mainly consists of pyroxene (39.4%), plagioclase (37.5%), olivine (9.8%), Fe-Ti oxides (1.9%), glass (8.3%) and other minor or trace phases. The results are consistent with previous analyses with larger sample sizes. In addition to minimum sample consumption, this method requires very little sample preparation, and can rapidly build a large database with each particle precisely traceable. Therefore, this novel technique is particularly suitable for the analysis of future returned soil samples from extraterrestrial bodies.

Keywords Raman-based particle analysis, Modal abundance, Size-dependent mineralogy, Laser-induced oxidation

Citation: Cao K, Dong M, She Z, Xiao Q, Wang X, Qian Y, Li Y, Wang Z, He Q, Wu X, Zong K, Hu Z, Xiao L. 2022. A novel method for simultaneous analysis of particle size and mineralogy for Chang'E-5 lunar soil with minimum sample consumption. Science China Earth Sciences, 65(9): 1704–1714, https://doi.org/10.1007/s11430-022-9966-5

1. Introduction

The mineral components of lunar soils and their characteristics are critical to understanding the source materials that have contributed to the regolith, as well as to interpreting remotely sensed data (Pieters et al., 2000). Since the 1970s, various techniques have been used to determine the mineral modes and particle size of the Apollo and Luna samples. For particle size analysis, various methods have been employed, such as the sieving methods (Carrier, 1973), image analysis coupled with scanning electron microscopy (Park et al., 2008) or optical microscopy (Li C et al., 2022), and laser diffractometer measurements (Zhang et al., 2022). For determining mineral constituents, the most widely used techniques include optical particle counts (McKay et al., 1974; Simon et al., 1982), X-ray diffraction (XRD) analysis

* Corresponding author (email: zbsher@cug.edu.cn)

(Taylor et al., 2019) and X-ray imaging (Taylor et al., 2001; Pieters et al., 2006). However, most of these methods require either a relatively large sample size or specific sample preparation, which are sometimes not possible because investigators are often required to work with exceptionally small amounts of samples, typically at the milligram level. Moreover, particle size information and mineral modes are usually independently obtained with different instruments, and are difficult to be correlated.

As the first lunar sample-return mission of China, Chang'E-5 landed in a young mare unit in northern Oceanus Procellarum (Qian et al., 2021), a previously unexplored area, and brought back to Earth a total weight of 1731 g lunar regolith on Dec. 17, 2020 (Deng et al., 2021; Zhou et al., 2022). Recent geochronological studies have anchored the age of the CE-5 samples at ~2.0 Ga (Che et al., 2021; Li et al., 2021), confirming that they are derived from late-stage mare basalts on the Moon. Therefore, the Chang'E-5 (CE-5) samples represent the only ground truth for the late-stage mare basalts (Staid et al., 2011; Zhang et al., 2016) which are critical for calibrations of orbital remote sensing data, provided that their mineral constituents are accurately determined. However, determining the mineral constitution with traditional methods typically requires relatively large sample amounts and leads to considerable sample consumption, which are usually not allowed for many planetary missions such as the Chang'E-5 and, in particular, asteroid sample returns (Watanabe et al., 2017). Moreover, it is the <45 μm fraction that dominates the spectral signature of the bulk lunar soil (Pieters et al., 1993, 2006), whereas traditional modal abundance analysis such as XRD do not provide any particle size information and thus may not be directly applied to the interpretation of orbital spectral data.

To tackle these problems, we developed a novel analytical technique that allows for simultaneous analyses of mineral constituents and particle size properties for the CE-5 soil sample with minimum sample consumption. This technique is based on confocal Raman spectroscopic system equipped with an automated particle analysis tool. We show that particle size properties and modal abundance of the CE-5 soil samples can be simultaneously and accurately determined with very small amounts of sample (μg level). Our data provide new insights into the mineral constitution of the CE-5 soil that can be directly compared with remote sensing data.

2. Samples and methods

A 200 mg aliquot of the 50-g fraction (CE5-C0400YJM00403) of the scooped CE-5 lunar soil, prepared by the National Astronomical Observatories of China (Li C et al., 2022), was obtained from China National Space Administration following The Procedures for Requesting Lunar Samples (http://www.cnsa.gov.cn/english/n6465645/n6465648/index.html). Subsamples were scooped with a clean mini-scoop from the original bottle in an anaerobic glove box and stored in carefully cleaned bottles for further analysis.

2.1 Sample preparation

Small aliquots (*ca*. 30 μg each) of the CE-5 soil sample were taken from the subsample bottles and placed on 75 mm× 25 mm Al-coated glass slides and then dispersed by impacting two to three drops of *ca*. 5 μL ultra-pure water to the soil with a micropipette (Figure 1a). The glass slides were then dried on a hot plate at 60°C. Prior to sample preparation, the tools were repeatedly cleaned with acetone, methanol and then ultra-pure water, whereas the Al-coated glass slides were also cleaned and checked in the dark field reflected light mode of the microscope to make sure there were no observable impurities on the surface. No organic solvent was used during the dispersion to minimize potential organic contamination. This method produces a good particle dispersion on the glass slides with only local occurrence of aggregation (Figure 1b).

2.2 Lunar soil particle analysis

Dispersed lunar soil particles were analyzed at the State Key Laboratory of Biogeology and Environmental Geology, China University of Geosciences (Wuhan) using the WITec α300R confocal Raman system equipped with the ParticleScout (v5.3.14.106) automated particle analysis tool. Large area image stitching and focus stacking were performed with 20× (N.A.=0.50) or 50× (N.A.= 0.80) dark field objectives (Figure 1b). Particles were automatically recognized from the obtained images based on their brightness, which allows the reconstruction of particle distribution maps (Figure 1b). Three NIST particle size standards (Duke Standards, Thermo Scientific) and two in-house standards were also analyzed, which yielded accuracy better than 1% for 10 and 100 μm particles, *ca*. 10–20% for 6 and 2 μm particles, and *ca*. 70% for 1 μm particles (Appendix Figure S1, Table S1; http://link.springer.com). The over-estimation of the sizes for small particles is likely due to overexposure during the dark-field imaging which is required to detect these particles, because their sizes approach the spatial resolution of the objectives used for imaging. Linear regression results of the five standards (Figure S1c–S1d) were used to construct calibration equations for measured particle sizes. For analysis of the CE-5 samples, particles with solidity >0.85 were selected to minimize the effect of particle aggregation (Table S2). The measured particle size data for CE-5 soil were calibrated, with statistical results presented in Table S3.

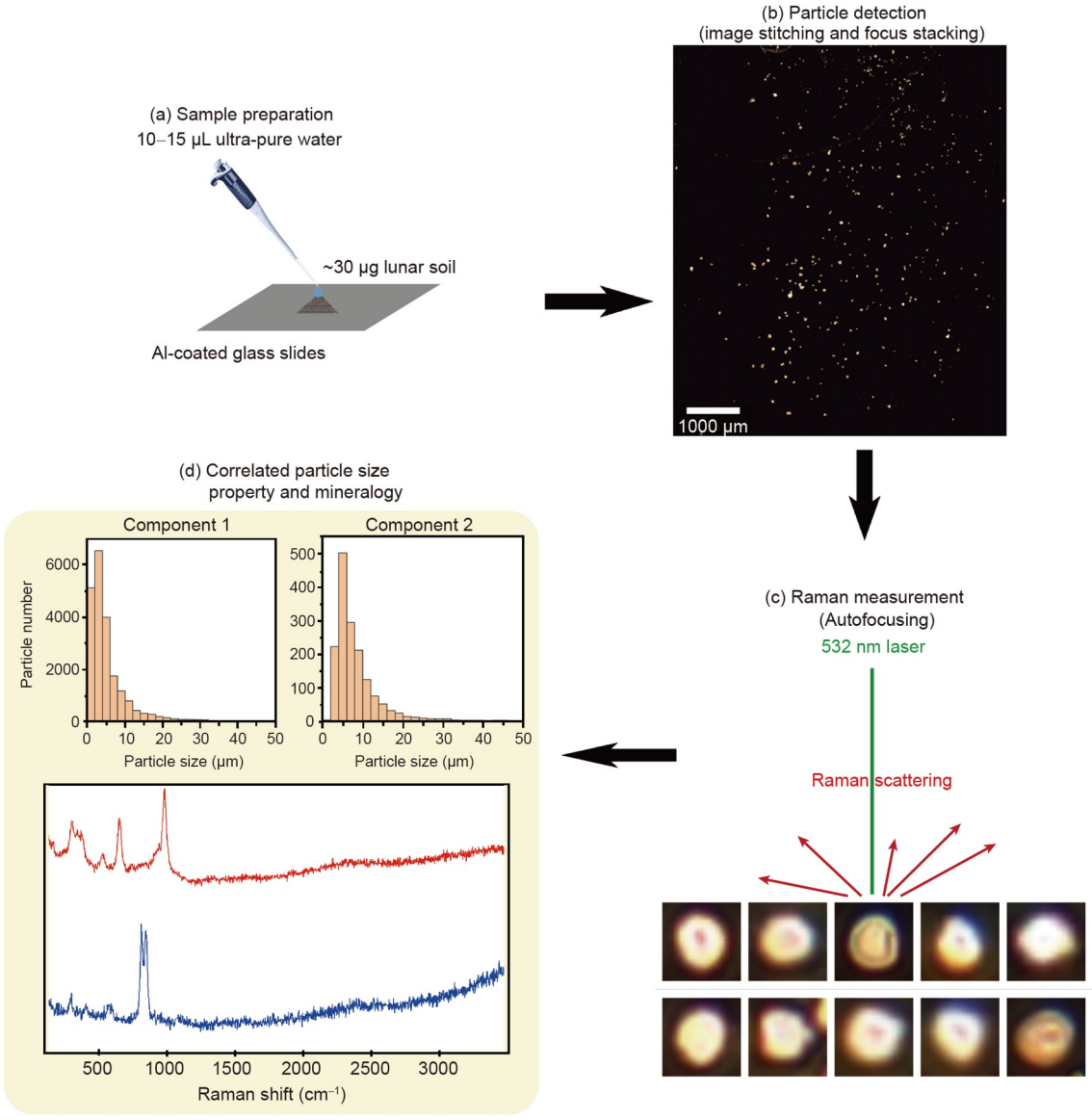

Figure 1 Simultaneous determination of particle size property and mineral constituents with automated Raman-based analysis.

For Raman analysis (Figure 1c), particles with grain sizes between 1 and 45 μm were selected. Automatic focusing was applied under the 50× (N.A.=0.80) dark field objectives during the analysis of each particle to obtain a spectrum with the highest signal to noise ratio (Figure 1d). A 532 nm laser was used with output laser power maintained at 3 mW. The integration time was set between 2 and 5 s with 5 to 8 accumulations to obtain spectra with a fair signal to noise ratio. In order to document laser-induced oxidation of opaque minerals, Fe-Ti oxides and Fe sulfide (FeS) in two grain mounts were also analyzed with progressively increasing laser power from 1 to 10 mW.

The documented phases include pyroxene, plagioclase, olivine, Fe-Ti oxides, Fe sulfide, glass and other minor or trace phases (e.g., phosphate and quartz). Model abundances of these phases were calculated based on the sum of their spherical equivalent volume ($V_{SE}=\pi\times(d_{CE}^3/6)$, where d_{CE} refers to the circular equivalent diameter of the particles.

2.3 Scanning electron microscopy

Scanning electron microscopy (SEM) was conducted in the State Key Laboratory of Biogeology and Environmental Geology, China University of Geosciences (Wuhan). Secondary electron and backscattered images were obtained with a Tescan VEGA 3 SEM or a Hitachi SU8010 field emission SEM, whereas energy dispersive spectroscopy (EDS) was performed with an Oxford Instrument AztecOne XT EDS detector attached to the Tescan SEM. Analyses were performed on the lunar soil particles under a vacuum pressure of 10^{-3} bar at 10–15 kV accelerating voltage, with working distances between 10 and 15 mm (1 bar=10^5 Pa). The samples

were coated with a nanometer layer of Au prior to analysis.

3. Results

3.1 Size distribution

Six analyses were performed on two dispersed samples (4-2 and 9-1) from the CE-5 soil (CE5C0400YJM00403), which gave consistent results of particle size distribution (Figure S2). When combined together, these analyses yield a dataset of 24881 particles. The particle size (circular equivalent diameter) ranges between 0.4 and 73.9 μm with a mean of 3.5 μm, a medium of 2.3 μm and a mode of 1.0 μm (Figure 2a, Table S3). The minimum Feret diameters are slightly smaller, varying between 0.4 and 66.0 μm (mean=3.0 μm). The CE-5 particles are typically irregular and slightly elongated, with a mean aspect ratio of 0.8 (Table S3).

The volume, defined as spherical equivalent volume (V_{SE}) of the particles, range between 0.04 and 211695 μm^3, with a medium of 6.5 μm^3 and a mean of 289.5 μm^3. The large standard deviation suggests that the particle volume is highly variable (Table S3). Although the majority of the particles have a small size (<6 μm), the >8 μm fraction accounts for >90% of the total volume (Figure 2b).

3.2 Raman spectral features and elemental composition

Typical Raman and EDS spectra for the recognized phases in the CE-5 soil are shown in Figure 3. Pyroxenes are characterized by two strong peaks in the 990–1000 cm^{-1} and 650–670 cm^{-1} spectral ranges, assigned as the symmetric stretching vibrations of the Si–O bond in [SiO_4] tetrahedra and the Si-O-Si bonds in $[Si_2O_6]_n$ chains, respectively (White, 1975). In addition, a group of peaks between 320 cm^{-1} and 390 cm^{-1} are also observed, likely produced by crystal lattice modes involving the displacement of cations and by the mixing of internal and external modes (Ghose et al., 1994). Although pyroxene is dominated by clinopyroxene (Cpx), trace amounts of orthopyroxene (Opx) are also observed, as characterized by an asymmetric peak at *ca.* 670 cm^{-1} as opposed to a symmetric one at *ca.* 660 cm^{-1} for Cpx. The asymmetricity of the 670 cm^{-1} peak for orthopyroxene reflects the presence of a shoulder on its lower frequency side that otherwise forms a separate peak around 660 cm^{-1} (Wang et al., 2001; Ling et al., 2011a). Plagioclase feldspars show prominent peaks around 510 cm^{-1}, which belong to the ring-breathing modes of the four-member tetrahedra of feldspars (Sharma et al., 1983). Olivine exhibits diagnostic doublets near 820 cm^{-1} and 850 cm^{-1}, attributed to the internal stretching vibrational modes of the SiO_4 ionic group (Chopelas, 1991).

Quartz and its polymorph cristobalite have the same elemental composition (Figure 3b) but show completely different Raman spectral patterns (Figure 3a) because they have distinct crystal structures. The most intense peaks occur in two regions, i.e., 350–500 cm^{-1} (O-Si-O bending modes), and <300 cm^{-1} (Si-O-Si bending and torsional/twisting modes) (Etchepare et al., 1974). Cristobalite has three predominant peaks around 418 cm^{-1}, 228 cm^{-1} and 112 cm^{-1}, whereas quartz peaks occur at 461 cm^{-1} and 123 cm^{-1} (Figure 3a). Apatite is characterized by an intense peak around 960 cm^{-1}, which corresponds to stretching vibrational modes of PO_4 tetrahedra (Jolliff et al., 2006). In addition, some apatites may exhibit additional, broad bands at 2069 cm^{-1} and 3278 cm^{-1} likely due to photoluminescence of rare earth elements (Gaft et al., 2005; Lenz et al., 2015). Hence, it is here termed as REE-apatite. Unlike the crystalline phases, glass does not show any well-defined peaks but instead exhibits a weak, broad band centered at *ca.* 960 cm^{-1} which can be assigned as the symmetric stretching vibrational mode of the $Si\text{-}O_{non\text{-}bridging}$ bond in a tetrahedron (McMillan, 1984).

3.3 Opaque phases

It is well known that opaque minerals such as Fe-Ti oxides, Fe sulfides and nanophase metallic iron (npFe0) in lunar soils may be oxidized during laser heating and produce altered Raman spectra. To assess the effects of laser-induced oxidation, we analyzed Fe-Ti oxides and Fe sulfides in polished grain mounts of CE-5 soil particles. The phases were firstly identified under the reflected light microscope and were subsequently analyzed with Raman spectroscopy to obtain reference spectra for comparison with those measured from unpolished particles dispersed on glass slides.

As shown in Figure 4, Fe-Ti oxides and Fe sulfides show distinct resistance to oxidizing alteration upon heating by the incident laser beam. Ilmenite is characterized by an intense peak near 680 cm^{-1} that likely corresponds to the bonds in (Cr^{3+}, Fe^{3+}, Al^{3+})O_6 octahedra (Wang et al., 2004), and subordinate peaks around 227 cm^{-1} and 330 cm^{-1} (Figure 4a). It remains largely unoxidized even with a relatively long duration of laser radiation (i.e., 60 s) when the laser power was kept below 5 mW. At 5 mW, the intensity of the main peaks for Fe-Ti oxide decreases, suggesting the onset of structural change due to oxidation. Further increase of laser power to 8 mW led to the disappearance of the peaks. The presence of Fe-Ti oxides is also confirmed by the high abundance of Ti and Fe shown in their EDS spectra (Figure 3b). These phases are typically <5 μm in diameter and occur as euhedral to subhedral, platy crystals (Figure S3).

Fe sulfide, in contrast, shows essentially no Raman signal under 1 mW laser power. Increase of laser power, however, led to the rapid oxidation of the Fe sulfide, as shown by the occurrence of magnetite-like peak (*ca.* 660 cm^{-1} at 2 mW) and subsequently hematite-like peaks (*ca.* 290, 400,

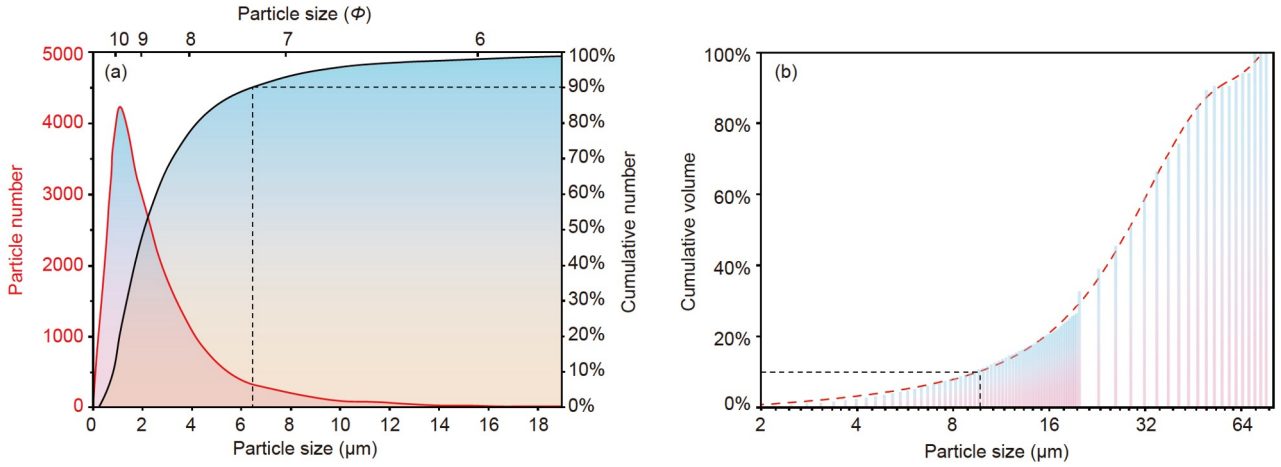

Figure 2 Size distribution of the CE-5 soil. (a) Curves of particle size distribution and cumulative number (%); (b) cumulative volume curve.

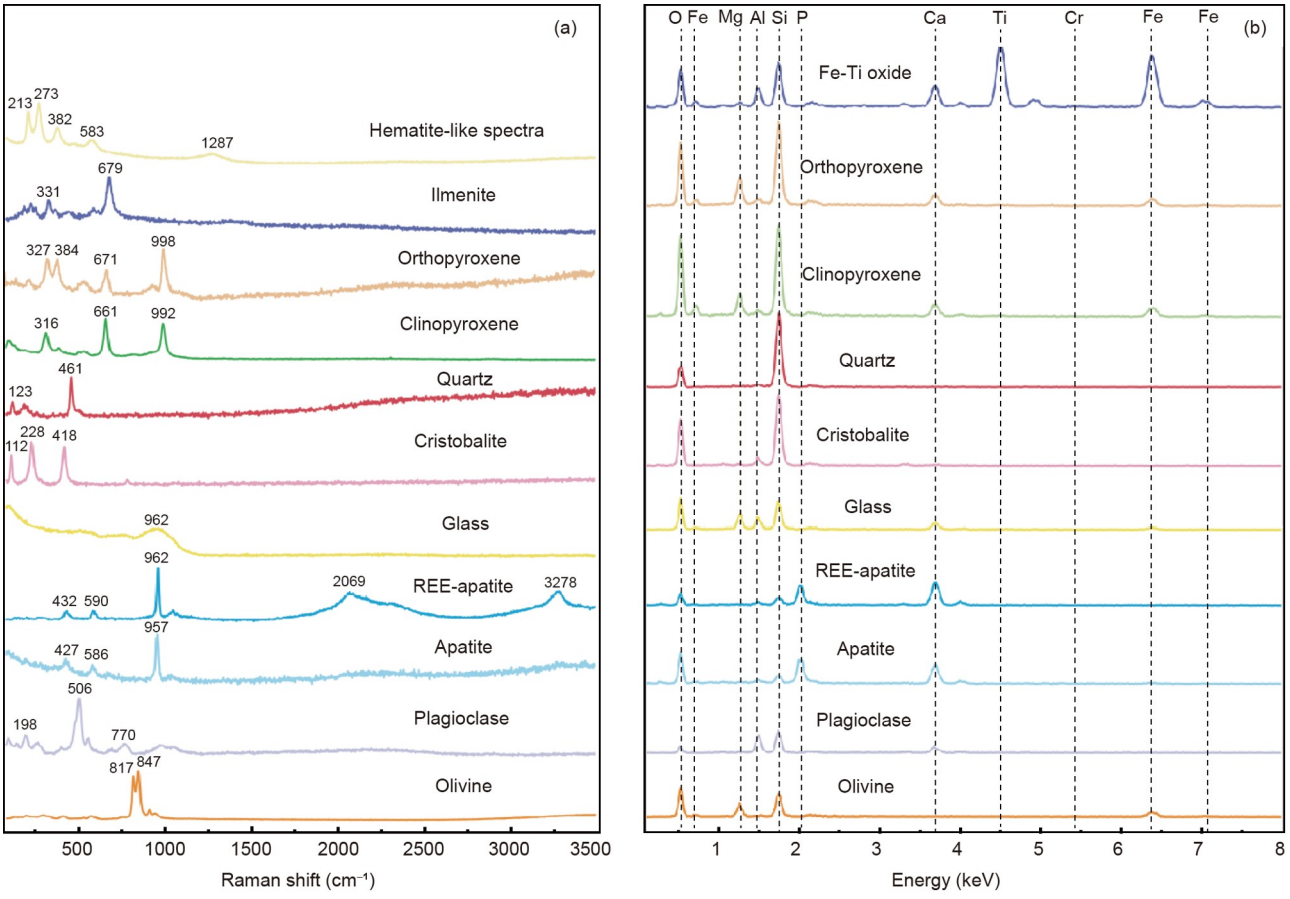

Figure 3 Representative Raman spectra (a) and EDS spectra (b) for various phases in the CE-5 soil.

1290 cm^{-1} from 2.5 mW) (Figure 4b).

It is also noted that lunar soil particles commonly contain npFe0, which might also be oxidized during laser heating. However, the nanometer size of these metal phases means that they are below the detection limit of optical microscopy and thus are difficult to be effectively documented with Raman spectroscopy. Nonetheless, it is expected that some hematite-like spectra could also represent oxidized npFe0. Considering the relatively low laser power used in this study, most Fe-Ti oxides would not be completely oxidized and display hematite-like spectra. Therefore, we attribute the hematite-like spectra to either Fe sulfide (troilite) or npFe0.

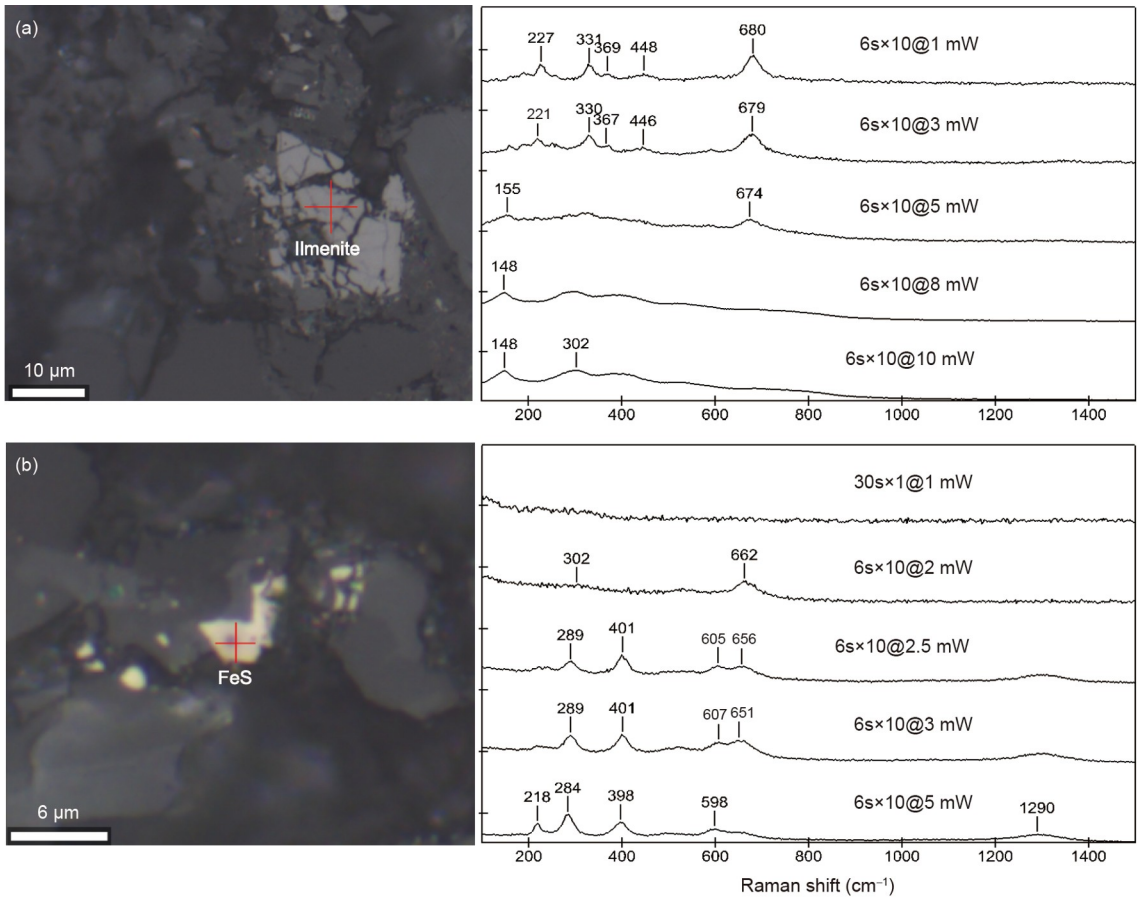

Figure 4 Reflected light images and Raman spectra of Fe-Ti oxide (a) and Fe sulfide (b) obtained with progressively increasing laser power.

3.4 Modal abundances

The Raman-based particle analysis system allows simultaneous determination of particle size properties and mineral constituents (Figures 5, S4–S5; Table S4), which is augmented by SEM-EDS analysis (Figures 3b, S3; Tables S5–S8). Typically, 35% to 40% of the analyzed particles were automatically identified as a mineral or glass, whereas the remaining ones are assigned as unidentified due to poor Raman signal or low HQI (hit quality index).

A total of 8070 particles have been identified by the six separate analyses (Figures S4, S5; Table S2). Among these, one analysis (Sample No. 9-1b) has been discarded considering the effect of mineral aggregation and fractionation during particle dispersion (Figure S5a). The remaining five analyses yield a total of 5927 identified particles, consisting of 39.4% pyroxene, 37.5% plagioclase, 9.8% olivine, 1.9% Fe-Ti oxides, 3.2% other mineral phases (Fe sulfide, npFe0, phosphate and silica) and 8.3% glass (Figure 5a, Table S4). It is noted that mineral constituents of different size fractions of the CE-5 soil show considerable variations (Figures 5b, S4, S5). In the largest fraction (20–45 μm), pyroxene is the most abundant phase (49%), followed by plagioclase (32%), olivine (11%) and glass (8%), while Fe-Ti oxides, phosphate and silica minerals are absent. With the decrease of particle size, the abundance of plagioclase increases, whereas that of pyroxene decreases dramatically (Figure 5b). Olivine content shows a similar, but less significant trend as that of pyroxene.

4. Discussion

4.1 Particle size and maturity

It has been proposed that the use of minimum Feret diameter (d_{FM}) is more appropriate than that of circular equivalent diameter (d_{CE}) when compared with particle size data obtained with traditional sieving methods (Zhang et al., 2021). However, our results show that d_{FM} values are only slightly smaller than d_{CE} values (Table S3), which would have minimal impact on comparisons. To be consistent with previously published data on the CE-5 samples, we use d_{CE} in the following discussion.

The high consistency of the 5 separate particle size datasets (Figure S2) demonstrates the homogeneous nature of the CE-5 sample. This is consistent with the fact that the scooped CE-5 samples have been thoroughly mixed and homo-

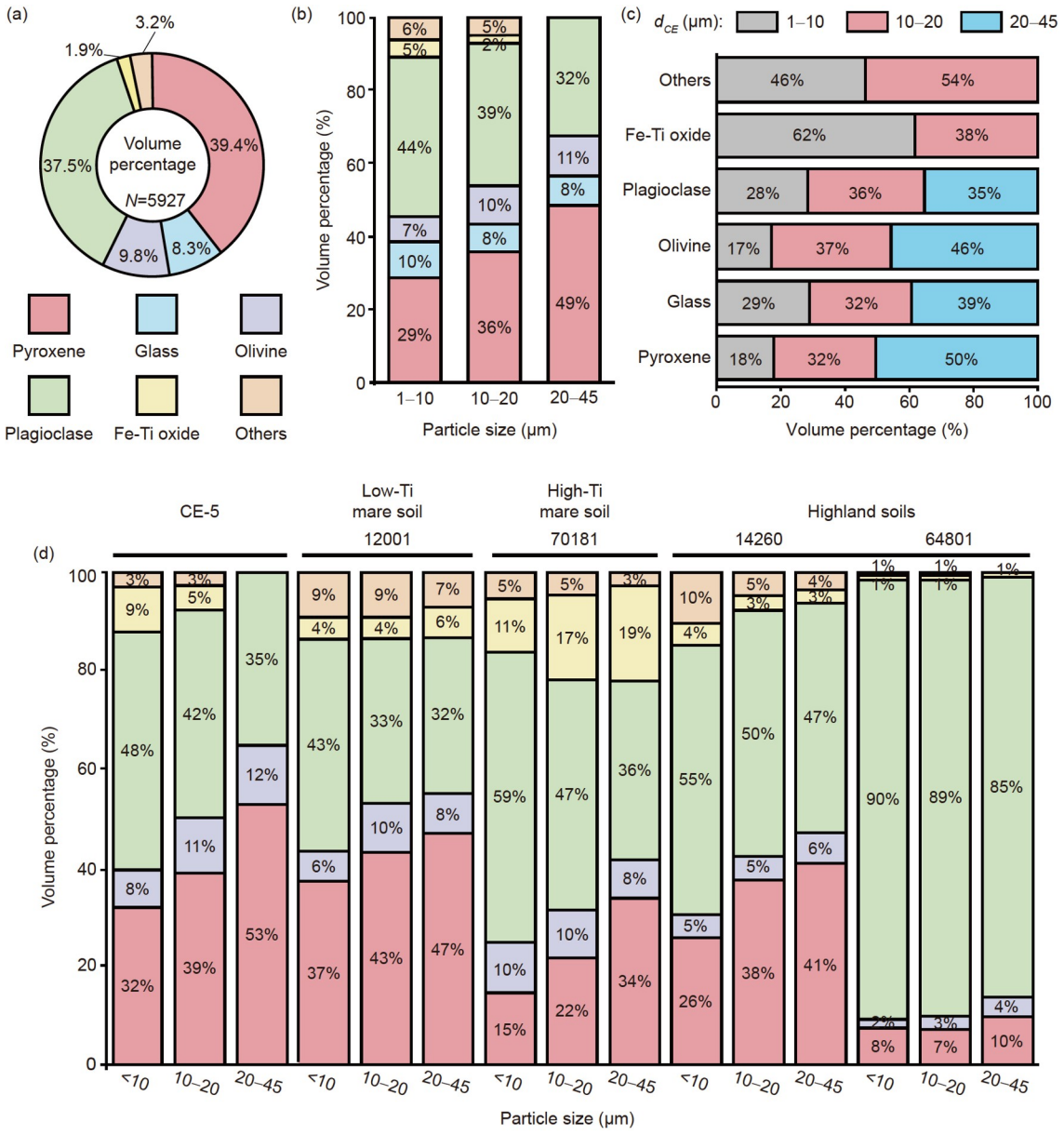

Figure 5 Modal abundances of the CE-5 soil ((a)–(c)) and comparison with typical Apollo soils (d). (a) Total volume percentages of various phases; (b) size-dependent mineral abundance; (c) relative abundances of various phases in different size fractions; (d) glass-free modal abundances of the CE-5 and Apollo soils. Data source: mare soils, Taylor et al. (2001); highland soils, Taylor et al. (2010).

genized in the laboratory (Li C et al., 2022). With only 24881 particles analyzed (~60 μg in total), our results (mean d_{CE}= 3.5 μm) generally agree with analysis of 299,869,867 particles in the size range of 1 to 500 μm (mean d_{CE}=3.96 μm; Li C et al., 2022). The unimodal distribution of the particle size for CE-5 soil (Figures 2, S2a–S2e) is consistent with those of the mature soil returned by the Apollo missions (Graf, 1993). Our analysis also yields significantly lower values of mode (peak of particle size distribution) and sorting than that obtained by Li C et al. (2022) and those for Apollo soils (Table S3, Figure S2f). This is probably due to the lower detection limit of our method that recognizes all particles > 0.4 μm, as determined by the diffraction limit of the 50×objective (N.A. =0.80). Regardless, our data suggest a high maturity for the CE-5 soil despite its young age, the origin of which demands further investigations.

As shown by Park et al. (2008), the Apollo 11 (Sample No. 10084) and 17 (Sample No. 70051) dust samples (<20 μm fraction) exhibit log-normal size distributions with peak modes in the range 100–300 nm, and contains ultrafine particles down to 20 nm. It is thus likely that most of the submicrometer particles in CE-5 soil have not been detected with the optical microscopy and can be documented by scanning electron microscopy in future studies.

4.2 Modal abundance and size-dependent mineralogy

Recent XRD analyses of three CE-5 soil samples (CE5C0800YJFM001, CE5C0800YJFM002 in Li C et al. (2022); CE5C0400 in Zhang et al. (2022)) show that they contain 29.1–31.8 wt% plagioclase, 39.7–44.5 wt% clinopyroxene (augite and pigeonite), 3.6–6.4 wt% olivine, 4.3–6.0 wt% ilmenite, 15.5–16.6 wt% glass, with minor amounts of other phases (0.5–1.8 wt% in total). Our analyses yield model (volume) abundance for the CE-5 soil sample (Figure 5a), which broadly agrees with the XRD data when converted into weight percentages (Table S4), although olivine abundance is significantly higher (12.2 wt%) whereas glass is much lower (6.8 wt%). The underestimation of glass abundance is understandable because glass has weaker Raman signals than crystalline minerals (Ling et al., 2011a). The high abundance of olivine is unexpected, although previous remote-sensed data have predicted elevated concentrations of olivine or iron-bearing glass in late-stage lunar basalts and soils at the CE-5 landing site (Staid et al., 2011; Qian et al., 2020). One possibility is that olivine is relatively over-represented in the lunar soil particles detectable with Raman spectroscopy (>1.0 μm). This is likely because olivine has been less affected by fining due to meteoroid impact, considering that it has poorer cleavages, as opposed to perfect cleavages for plagioclase and pyroxene, and greater Mohs hardness (6.5–7.0) than the other major phases (6–6.5 for plagioclase and 5.5–6.0 for augite). Furthermore, olivine abundance might have been overestimated by the Raman analyses, because they generally have a stronger Raman signal compared to most of the other phases. In any case, further investigations are needed to determine the actual abundance of olivine in the CE-5 soils.

It is notable that the mineral constituents of the CE-5 soil are size-dependent, as featured by the preferential concentration of olivine and pyroxene in contrast to the depletion of plagioclase in coarser fractions (Figure 5b, 5c). This agrees with previous studies on Apollo soils that documented generally decreasing trends for pyroxene and olivine and an increasing trend for plagioclase in progressively fining fractions (Figure 5d; Taylor et al., 2001, 2010). These trends are likely produced by preferential comminution of plagioclase over mafic minerals during space weathering (i.e., meteoroid impacts), as experimentally verified by Cintala and Hörz (1992). In general, the CE-5 soil is most similar to low-Ti mare soils in terms of mineral constituents (Figure 5d), consistent with bulk geochemical results (Li C et al., 2022).

It has been suggested that the 10–20 and 20–45 μm size fractions are the most similar to the bulk lunar soil, whereas larger size fractions are not representative of bulk soil properties (Pieters et al., 1993; Fischer, 1995). Moreover, it is the <45 μm particle-size domains of the lunar soil that appear to dominate the spectral signature of the bulk soil (Pieters et al., 1993, 2006). Our results provide the first estimate of mineral constituents for the 1–45 μm fractions of the CE-5 soil and thus is most useful for analysis of the *in-situ* CE-5 Lunar Mineralogical Spectrometer data (Zhou et al., 2022) and furthermore as the ground truth of the landing site for remotely sensed data.

4.3 Minor phases in CE-5 soil

The presence of a variety of accessary minerals, including Ca-phosphate, chromite, troilite, baddeleyite, zirconolite, silica and K-feldspar phases, have been documented in the CE-5 soil and basalt clasts (Che et al., 2021; Jiang et al., 2022; Li C et al., 2022). Most of these phases are also found with Raman spectroscopy in this work (Figure 3a). The estimated total modal abundance (3.2%) for the minor phases is generally consistent with those determined with electron probe micro-analyzer (EPMA) on the CE-5 basaltic clasts (Che et al., 2021; Jiang et al., 2022). As an advantage of Raman spectroscopy, polymorphs such as cristobalite and quartz are easily distinguished (Figure 3a). Our results show that the two silica polymorphs have the same abundances in the analyzed CE-5 soils (Table S4), although it has been argued that cristobalite is more abundant and can constitute up to 5 vol% of some mare basalts (Papike et al., 1998).

In previous studies, orthopyroxene has not yet been reported from CE-5 samples, while EPMA analyses have shown that the CE-5 pyroxenes are predominantly augite with an average composition of $Wo_{32.9}En_{28.2}Fs_{38.9}$, with rare pigeonite (e.g., Jiang et al., 2022; Li C et al., 2022). The detection of minor amounts of orthopyroxene in the present study suggest that the CE-5 soil probably contains very limited highland material, as orthopyroxene is a common constituent (up to 7.6%) in Apollo highland soils (Taylor et al., 2010). Although the origin of orthopyroxene in the CE-5 soil remains to be explored, it is of great importance because orthopyroxene contains lower calcium and show distinct spectral features compared with that of clinopyroxene in remote sensed data (Zhou et al., 2022). Therefore, further investigations should pay attention to the presence of orthopyroxene in the CE-5 samples.

4.4 Simultaneous determination of particle size and mineralogy with Raman-based particle analysis: A promising technique for studies of extraterrestrial soils

Determination of the particle size and mineral constituents of the lunar soils has been a long endeavor since the first lunar sample return mission (e.g., Duke et al., 1970; Li C et al., 2022). With the requirement of very small sample consumption when analyzing the CE-5 soil, however, many traditional techniques (e.g., XRD) may not be applicable.

Without properly polished surfaces, the constituents of fine lunar particles cannot be accurately determined by EPMA. Recently, relatively new techniques such as μ-XRF, high resolution X-ray tomographic microscopy (HR-XRTM) have also been used to determine the mineralogy of lunar soils (e.g., Jiang et al., 2022; Li J H et al., 2022). While X-ray microcomputed tomography (micro-CT) and the latest X-ray tomographic microscopy (XRTM) can reveal the 3D mineralogy of a single lunar soil particle at a micron-scale resolution (Jiang et al., 2022), analysis of large amounts of particles would be extremely time-consuming. In contrast, μ-XRF has the ability to rapidly determine the elemental composition of particles (Li J H et al., 2022), although no information on molecular structure is provided for distinguishing polymorphs or phases with similar elemental composition.

Micro-Raman spectroscopy is a non-destructive analytical technique, which has been widely used to characterize the molecular structure of various kinds of materials including minerals. A number of previous studies have employed the Raman point count (RPC) method to determine the mineral constitution of the Apollo lunar soils (Wang et al., 1995; Haskin et al., 1997; Israel et al., 1997; Ling et al., 2011a, 2011b), which have shown the great potential of this technique (Ling et al., 2011b). However, reported RPC datasets generally contain less than 200 grains for each sample, while no particle size information has been obtained (e.g., Haskin et al., 1997; Ling et al., 2011a).

The Raman-based particle analysis technique employed in this study, in contrast, can automatically analyze thousands of lunar soil particles within one day, and generate datasets with correlated particle size property and Raman spectra (and thus compositional information) for each particle (Figures 5, S4, S5). Moreover, all particles are traceable and can be checked with further Raman or SEM-EDS analysis. This method not only allows for the build-up of a large database in a relatively short period of time, but also facilitates discovery of rare phases such as orthopyroxene, phosphates and silica minerals as shown in this work, which would be difficult, if not impossible, to be identified by traditional methods such as XRD. With proper sample transfer methods, these particles can be made available for further analysis with various state-of-the-art *in situ* micro-analytical techniques.

It should be noted that, as previously pointed out for the Raman point count method, the abundance of glass tends to be underestimated due to their weak Raman signal (Ling et al., 2011a). This is likely also the case for opaque minerals such as ilmenite, because they have lower strength in Raman signals than pyroxene and olivine (Ling et al., 2011a). Furthermore, detection of Raman inactive phases, such as shocked anorthite that commonly exists in lunar soils, needs to be augmented by other techniques such as EPMA. Lastly, the present Raman-based particle analysis does not provide information on mineral modes in multi-phase particles and agglutinates, because it collects only one spectrum for each particle. However, we show that, with sufficiently large numbers of particles (n >5000) analyzed, this method yields a good estimation of mineral modes generally consistent with the results of XRD analyses with large sample amounts (Li C et al., 2022; Zhang et al., 2022).

In summary, the Raman-based particle analysis method has the advantages of low sample consumption (~30 μg per analysis), high efficiency and the ability of simultaneous acquisition of multi-dimensional information for micrometer-sized particles. Therefore, it has great potential for future studies of soil samples returned from extraterrestrial bodies, such as the Moon, Mars and asteroids. Further improvements of this method may include (1) development of simulated lunar soil standards with various mineral constituents; (2) establishment of a comprehensive Raman database for all phases in the lunar samples; (3) enhancement of identification rate for phases with weak Raman signal; and (4) improvement of analytical protocol for better representation of multi-phase particles.

5. Summary

Six subsamples from two aliquots of the CE-5 soil sample were analyzed for particle size and mineral constituents with a Raman-based particle analysis system. The CE-5 soil sample has an overall small size (mean=3.5 μm) and a unimodal particle size distribution, indicating a high maturity. Raman analysis of 5927 particles in the size range of 1 to 45 μm yielded a modal abundance of 39.4% pyroxene, 37.5% plagioclase, 9.8% olivine, 1.9% Fe-Ti oxides and 8.3% glass, which is in general agreement with previous XRD analyses with much larger sample sizes. The analyses also reveal the presence of orthopyroxene, quartz, cristobalite and apatite, and documented the preferential concentration of olivine and pyroxene in contrast to the depletion of plagioclase in coarser fractions of the CE-5 soil. Our data provide the first estimate of mineral constituents for the 1–45 μm fraction of the CE-5 soil and thus can be used to interpret the *in situ* and orbital remote sensing data.

The Raman-based particle analysis method requires minimum sample consumption (magnitudes lower than traditional methods), very little sample preparation, and can rapidly build large, correlated particle size and Raman spectral datasets with each particle traceable. The resultant large databases also facilitate the discovery of rare mineral phases of interest. Further development of this novel technique will ensure rapid analysis of future returned soil samples from other extraterrestrial bodies.

Acknowledgements *We are grateful to all staff of the Chang'E-5*

mission for their efforts that makes this work possible. The sample used in this study was provided by the China National Space Administration. We thank Hao YANG for assistance in SEM analysis, Dominic PAPINEAU for helpful discussions, Xiong XIONG for providing the NIST standards, and Hailong HU and Wanghua WU for technical support. We also acknowledge the insightful comments of two anonymous reviewers that helped improve the manuscript. This work was supported by the Pre-Research Project on Civil Aerospace Technologies funded by CNSA (Grant No. D020205), the National Natural Science Foundation of China (Grant No. 42172337), and the Program of the State Key Laboratory of Biogeology and Environmental Geology, China University of Geosciences (Grant No. GBL12101).

References

Anand M, Taylor L A, Misra K C, Demidova S I, Nazarov M A. 2003. KREEPy lunar meteorite Dhofar 287A: A new lunar mare basalt. Meteoritics Planet Sci, 38: 485–499

Carrier W D. 1973. Lunar soil grain size distribution. Moon, 6: 250–263

Che X, Nemchin A, Liu D, Long T, Wang C, Norman M D, Joy K H, Tartese R, Head J, Jolliff B, Snape J F, Neal C R, Whitehouse M J, Crow C, Benedix G, Jourdan F, Yang Z, Yang C, Liu J, Xie S, Bao Z, Fan R, Li D, Li Z, Webb S G. 2021. Age and composition of young basalts on the Moon, measured from samples returned by Chang'E-5. Science, 374: 887–890

Chopelas A. 1991. Single crystal Raman spectra of forsterite, fayalite, and monticellite. Am Miner, 76: 1101–1109

Cintala M J, Hörz F. 1992. An experimental evaluation of mineral-specific comminution. Meteoritics, 27: 395–403

Deng X J, Zheng Y H, Jin S Y, Yao M, Zhao Z H, Li H L, Jiang S Q, Wang G X. 2021. Design and implementation of sampling, encapsulating, and sealing system of Chang'E-5. Sci Sin-Tech, 51: 753–762

Duke M B, Woo C C, Bird M L, Sellers G A, Finkelman R B. 1970. Lunar soil: Size distribution and mineralogical constituents. Science, 167: 648–650

Etchepare J, Merian M, Smetankine L. 1974. Vibrational normal modes of SiO_2. I. α and β quartz. J Chem Phys, 60: 1873–1876

Fischer E M. 1995. Quantitative compositional analysis of the lunar surface from reflectance spectroscopy: Iron, aluminum, and model for removing the optical effects of space weathering. Doctoral Dissertation. Brown University

Gaft M, Reisfeld R, Panczer G. 2005. Modern Luminescence Spectroscopy of Minerals and Materials. New York: Springer. 356

Graf J C. 1993. Lunar soils grain size catalog. NASA Ref. Pub. 1265

Ghose S, Choudhury N, Chaplot S L, Pal Chowdhury C, Sharma S K. 1994. Lattice dynamics and Raman spectroscopy of protoenstatite $Mg_2Si_2O_6$. Phys Chem Miner, 20: 469–477

Haskin L A, Wang A, Rockow K M, Jolliff B L, Korotev R L, Viskupic K M. 1997. Raman spectroscopy for mineral identification and quantification for *in situ* planetary surface analysis: A point count method. J Geophys Res, 102: 19293–19306

Israel E J, Arvidson R E, Wang A, Pasteris J D, Jolliff B L. 1997. Laser Raman spectroscopy of varnished basalt and implications for *in situ* measurements of Martian rocks. J Geophys Res, 102: 28705–28716

Jiang Y, Li Y, Liao S, Yin Z, Hsu W. 2022. Mineral chemistry and 3D tomography of a Chang'E 5 high-Ti basalt: Implication for the lunar thermal evolution history. Sci Bull, 67: 755–761

Jolliff B L, Hughes J M, Freeman J J, Zeigler R A. 2006. Crystal chemistry of lunar merrillite and comparison to other meteoritic and planetary suites of whitlockite and merrillite. Am Miner, 91: 1583–1595

Lenz C, Nasdala L, Talla D, Hauzenberger C, Seitz R, Kolitsch U. 2015. Laser-induced REE^{3+} photoluminescence of selected accessory minerals — An "advantageous artefact" in Raman spectroscopy. Chem Geol, 415: 1–16

Li C, Hu H, Yang M F, Pei Z Y, Zhou Q, Ren X, Liu B, Liu D, Zeng X, Zhang G, Zhang H, Liu J, Wang Q, Deng X, Xiao C, Yao Y, Xue D, Zuo W, Su Y, Wen W, Ouyang Z. 2022. Characteristics of the lunar samples returned by the Chang'E-5 mission. Natl Sci Rev, 9: nwab188

Li J H, Li Q L, Zhao L, Zhang J H, Tang X, Gu L X, Guo Q, Ma H X, Zhou Q, Liu Y, Liu P Y, Qiu H, Li G, Gu L, Guo S, Li C L, Li X H, Wu F Y, Pan Y X. 2022. Rapid screening of Zr-containing particles from Chang'E-5 Lunar soil samples for isotope geochronology: Technical roadmap for future study. Geosci Front, 13: 101367

Li Q L, Zhou Q, Liu Y, Xiao Z, Lin Y, Li J H, Ma H X, Tang G Q, Guo S, Tang X, Yuan J Y, Li J, Wu F Y, Ouyang Z, Li C, Li X H. 2021. Two-billion-year-old volcanism on the Moon from Chang'E-5 basalts. Nature, 600: 54–58

Ling Z C, Wang A, Jolliff B L. 2011a. Mineralogy and geochemistry of four lunar soils by laser-Raman study. Icarus, 211: 101–113

Ling Z, Wang A, Jolliff B L. 2011b. A systematic spectroscopic study of four Apollo lunar soils. J Earth Sci, 22: 578–585

McKay D S, Fruland R M, Heiken G H. 1974. Grain size distribution as an indicator of the maturity of lunar soils. Proc Lunar Planet Sci Conf, 5: 480–482

McMillan P. 1984. Structural studies of silicate glasses and melts—Applications and limitations of Raman spectroscopy. Am Miner, 69: 622–644

Papike J J, Ryder G, Shearer C K. 1998. Lunar samples. In: Papike J J, ed. Planetary Materials, Reviews in Mineralogy. Mineralogical Society of America, Washington. 5-1–5-234

Park J, Liu Y, Kihm K D, Taylor L A. 2008. Characterization of lunar dust for toxicological studies. I: Particle size distribution. J Aerosp Eng, 21: 266–271

Pieters C, Shkuratov Y, Kaydash V, Stankevich D, Taylor L. 2006. Lunar soil characterization consortium analyses: Pyroxene and maturity estimates derived from Clementine image data. Icarus, 184: 83–101

Pieters C M, Taylor L A, Noble S K, Keller L P, Hapke B, Morris R V, Allen C C, McKAY D S, Wentworth S. 2000. Space weathering on airless bodies: Resolving a mystery with lunar samples. Meteoritics Planet Sci, 35: 1101–1107

Pieters C M, Fischer E M, Rode O, Basu A. 1993. Optical effects of space weathering: The role of the finest fraction. J Geophys Res, 98: 20817–20824

Qian Y, Xiao L, Yin S, Zhang M, Zhao S, Pang Y, Wang J, Wang G, Head J W. 2020. The regolith properties of the Chang'E-5 landing region and the ground drilling experiments using lunar regolith simulants. Icarus, 337: 113508

Qian Y, Xiao L, Wang Q, Head J W, Yang R, Kang Y, van der Bogert C H, Hiesinger H, Lai X, Wang G, Pang Y, Zhang N, Yuan Y, He Q, Huang J, Zhao J, Wang J, Zhao S. 2021. China's Chang'E-5 landing site: Geology, stratigraphy, and provenance of materials. Earth Planet Sci Lett, 561: 116855

Sharma S K, Simons B, Yoder H S. 1983. Raman study of anorthite, calcium Tschermak's pyroxene, and gehlenite in crystalline and glassy states. Am Miner, 68: 1113–1125

Simon S B, Papike J J, Laul J C. 1982. The lunar regolith-Comparative studies of the Apollo and Luna sites. Petrology of soils from Apollo 17, Luna 16, 20, and 24. Proc Lunar Planet Sci Conf, 12: 371–388

Staid M I, Pieters C M, Besse S, Boardman J, Dhingra D, Green R, Head J W, Isaacson P, Klima R, Kramer G, Mustard J M, Runyon C, Sunshine J, Taylor L A. 2011. The mineralogy of late stage lunar volcanism as observed by the Moon Mineralogy Mapper on Chandrayaan-1. J Geophys Res, 116: E00G10

Taylor G J, Martel L M V, Lucey P G, Gillis-Davis J J, Blake D F, Sarrazin P. 2019. Modal analyses of lunar soils by quantitative X-ray diffraction analysis. Geochim Cosmochim Acta, 266: 17–28

Taylor L A, Pieters C M, Keller L P, Morris R V, McKay D S. 2001. Lunar mare soils: Space weathering and the major effects of surface-correlated nanophase Fe. J Geophys Res, 106: 27985–27999

Taylor L A, Pieters C, Patchen A, Taylor D H S, Morris R V, Keller L P, McKay D S. 2010. Mineralogical and chemical characterization of lunar highland soils: insights into the space weathering of soils on airless bodies. J Geophys Res, 115: E02002

Tian H C, Wang H, Chen Y, Yang W, Zhou Q, Zhang C, Lin H L, Huang C,

Wu S T, Jia L H, Xu L, Zhang D, Li X G, Chang R, Yang Y H, Xie L W, Zhang D P, Zhang G L, Yang S H, Wu F Y. 2021. Non-KREEP origin for Chang'E-5 basalts in the Procellarum KREEP Terrane. Nature, 600: 59–63

Wang A, Jolliff B L, Haskin L A. 1995. Raman spectroscopy as a method for mineral identification on lunar robotic exploration missions. J Geophys Res, 100: 21189–21199

Wang A, Jolliff B L, Haskin L A, Kuebler K E, Viskupic K M. 2001. Characterization and comparison of structural and compositional features of planetary quadrilateral pyroxenes by Raman spectroscopy. Am Miner, 86: 790–806

Wang A, Kuebler K E, Jolliff B L, Haskin L A. 2004. Raman spectroscopy of Fe-Ti-Cr-oxides, case study: Martian meteorite EETA79001. Am Miner, 89: 665–680

Watanabe S, Tsuda Y, Yoshikawa M, Tanaka S, Saiki T, Nakazawa S. 2017. Hayabusa2 mission overview. Space Sci Rev, 208: 3–16

White W B. 1975. Structural interpretation of lunar and terrestrial minerals by Raman spectroscopy. In: Karr Jr. C, ed. Infrared and Raman Spectroscopy of Lunar and Terrestrial Minerals. New York: Academic Press. 325–358

Zhang H, Zhang X, Zhang G, Dong K, Deng X, Gao X, Yang Y, Xiao Y, Bai X, Liang K, Liu Y, Ma W, Zhao S, Zhang C, Zhang X, Song J, Yao W, Chen H, Wang W, Zou Z, Yang M. 2022. Size, morphology, and composition of lunar samples returned by Chang'E-5 mission. Sci China-Phys Mech Astron, 65: 229511

Zhang X, Wu Y, Ouyang Z, Bugiolacchi R, Chen Y, Zhang X, Cai W, Xu A, Tang Z. 2016. Mineralogical variation of the late stage mare basalts. J Geophys Res-Planets, 121: 2063–2080

Zhang Y, Jia J, Wang X, Chen J, van der Glas H W. 2021. Particle size distributions following chewing: Transformation of two-dimensional outcome from optical scanning to volume outcome from sieving. J Food Eng, 309: 110663

Zhou C, Jia Y, Liu J, Li H, Fan Y, Zhang Z, Liu Y, Jiang Y, Zhou B, He Z, Yang J, Hu Y, Liu Z, Qin L, Lv B, Fu Z, Yan J, Wang C, Zou Y. 2022. Scientific objectives and payloads of the lunar sample return mission—Chang'E-5. Adv Space Res, 69: 823–836

(Responsible editor: Hejiu HUI)